The 8th European Congress on Computational Methods in Applied Sciences and Engineering
ECCOMAS Congress 2022
5-–9 June 2022, Oslo, Norway

# IMMERSED BOUNDARY ANALYSIS OF MODELS WITH INTERNAL STATE VARIABLES: APPLICATIONS TO HYDROGELS

**JORGE L. BARRERA[1] AND KURT K. MAUTE[2]**

[1] Computational Engineering Division, Lawrence Livermore National Laboratory,
7000 East Ave, Livermore, California 94550, United States of America
email: barrera@llnl.gov

[2] Department of Aerospace Engineering Sciences, University of Colorado at Boulder,
3775 Discovery Driver, Boulder, Colorado 80303, United States of America
email: maute@colorado.edu

**Key words:** Immersed Analysis, XFEM, CutFEM, Internal State Variable, Hydrogels

**Abstract.** Research on Soft Active Materials (SAMs) has flourished in recent years driven mainly by potential applications to actuation systems, tissue engineering, and soft robotics. These applications benefit from the unique properties of SAMs such as large deformations, a wide range of stimulants, and high motion complexities. Hydrogels are among the dominant members of SAMs. Their highly nonlinear chemo-mechanical transient behavior is described by equations that include rates of internal state variables representing the local swelling state of the gel. Hence, the simulation of hydrogels requires intricate numerical approaches with stabilization schemes. This paper presents an immersed boundary analysis technique to simulate models with internal state variables. A hydrogel model is used as an example to describe the components of the proposed technique. Level sets define the material layout on a fixed background mesh and a generalized version of the extended finite element method predicts the response. The influence of the internal state variables on the stability of the physical analysis is examined. While focusing on an XFEM approach for hydrogels, the presented theory can be extrapolated to similar applications using models with internal state variables (e.g., shape memory polymers) and other immersed boundary analysis technique (e.g., CutFEM).

## 1 INTRODUCTION

Predicting realistic structural responses often requires accounting for intricate physical processes occurring locally within the material. Such models introduce a set of unknowns, labeled as *internal* state variables (ISVs), in addition to the state variables that describe the observable behavior like temperature or displacement. These ISVs model, for example, path-dependent material behavior and dissipative mechanisms that can be measured (e.g., average of microscopic effects, local structural rearrangement) ([1]). In this paper, we focus on the computational aspects and the implementation of models with ISVs in immersed boundary analysis techniques. These techniques capture crips interfaces on nonconforming meshes while providing accurate prediction of the response.

Models for Soft Active Materials (SAMs) can utilize ISVs to capture their slow time-dependent, highly nonlinear diffusive response produced by their intricate internal structures. Transient models for active materials such as gels (e.g., hydrogels, oil-based gels, aerogels) that can predict large deformations and complex motions are a notable example in this group; see, for example, [3, 4]. Models in which constitutive equations incorporate gradient-independent ISVs are defined by only the local values of the ISVs but not their spatial gradients and thus, lack stringent spatial continuity requirements. This feature is advantageous for Galerkin-based techniques such as the finite element method since the ISVs can be approximated pointwise/locally ([2]). In contrast, the governing equations of the observable response involve the spatial gradients of the state variables which leads to a globally coupled system of discretized equations.

Numerous publications have provided detailed implementations schemes for models with ISVs ([5, 6]). Most of the published work, however, focuses on standard finite element methods using a geometry conforming discretization due to its popularity and availability in commercial software. Limited research has considered immersed boundary analysis techniques. Moreover, contributions that use these techniques seldom elaborate on the computational aspects of their implementations ([7]).

This paper presents a simple alternative to discretize the ISVs in immersed boundary analysis techniques. In the proposed approach, the ISV variables do not depend on intersection patterns. In addition, weakly enforced boundary and interface conditions, as well as a stabilization technique, are augmented to include the influence of the ISVs in their formulations. To highlight the effectiveness of the proposed approach in simulating complex but relevant models, a coupled diffusion large deformation theory for the simulation of hydrogel is used [6]. The domain is discretized via the eXtended Finite Element Method (XFEM) in 3D examples.

This manuscript is organized as follows. Section 2 introduces the geometry description method together with a summary of a transient nonlinear hydrogel model. Section 3 details the discretization technique. The numerical approach to solve models with gradient-independent ISVs is summarized in Section 4. The examples of Section 5 demonstrate that the proposed handling of ISVs can reliably reproduce the hydrogel physical response, and Section 7 provides a set of conclusions and directions for future work.

## 2 MODEL PROBLEM

### 2.1 Domain description

Consider a domain $\Omega \subset \mathbb{R}^d$ for $d$ spatial dimensions composed of two material phases $\Omega^I$ and $\Omega^{II}$. The computational domain $\Omega$ is the union of these two non-overlapping partitions with boundaries $\partial\Omega^I$ and $\partial\Omega^{II}$ such that $\Omega = \Omega^I \cup \Omega^{II}$. External boundaries with prescribed Dirichlet and Neumann conditions are denoted by $\Gamma_D^m = \partial\Omega^m \cap \partial\Omega_D$ and $\Gamma_N^m = \partial\Omega^m \cap \partial\Omega_N$, respectively, with $m = [I, II]$. A crisp material interface, $\Gamma_{I,II} \subset \mathbb{R}^{d-1}$, defined as $\Gamma_{I,II} = \partial\Omega^I \cap \partial\Omega^{II}$, is described using a level set method ([8]). Thus, $\Gamma_{I,II}$ is defined by an isocontour of a level set function $\psi(\boldsymbol{X})$: $\psi(\boldsymbol{X}) < 0, \forall\ \boldsymbol{X} \in \Omega^I$; $\psi(\boldsymbol{X}) > 0, \forall\ \boldsymbol{X} \in \Omega^{II}$; and $\psi(\boldsymbol{X}) = 0, \forall\ \boldsymbol{X} \in \Gamma_{I,II}$; where $\boldsymbol{X}$ represents a point in the domain, as seen on the left side of Figure 2. Structured meshes composed of eight-node hexahedra are used to linearly interpolate the level set field.

### 2.2 Hydrogel coupled diffusion and large deformation theory

A transient nonlinear coupled chemo-mechanical hydrogel model that includes ISVs in rate form and is suitable for large deformations is introduced in this section. The material is assumed to be isotropic and defined by a Helmholtz free energy function, $\Upsilon$. For detailed derivations of the model presented below the reader is referred to [4, 6].

#### 2.2.1 Kinematic equations

Consider a dry macroscopically homogeneous elastomeric body in $\Omega^I$ in a fixed reference configuration. Let $\mathbf{x}$ be an arbitrary material point of $\Omega^I$. The motion of $\boldsymbol{x}$ in $\Omega^I$ is a smooth one-to-one mapping $\mathbf{x} = \tau(\mathbf{X}, t)$, with the deformation gradient defined as $\boldsymbol{F} = \nabla\tau$. The deformation gradient $\boldsymbol{F}$ is decomposed into elastic and swelling parts, i.e., $\boldsymbol{F}^e$ and $\boldsymbol{F}^s$, respectively, by a multiplicative decomposition $\boldsymbol{F} = \boldsymbol{F}^e\boldsymbol{F}^s$, with $\boldsymbol{F}^s = \lambda^s\mathbf{1}$. The swelling stretch, $\lambda^s > 0$, is given by $\lambda^s = \phi^{-1/3}$. The polymer volume fraction, $\phi$, is the single ISV in this model, defined by $\phi = \frac{1}{1+\Pi C_R}$, with $\Pi$ denoting the volume of a mole of fluid molecules, and $C_R$ representing the fluid concentration of the dry elastomer.

#### 2.2.2 Constitutive equations

The following free energy function accounts for the combined effects of mixing, swelling, and elastic stretching (see [4]):

$$\Upsilon = \left(\frac{1-\phi}{\phi\ \Pi}\right)\left[\mu^0 + (log(1-\phi) + \chi\phi)\,RT\right] + G\left[\frac{1}{2}tr(\boldsymbol{F}^T\boldsymbol{F}) - \frac{3}{2} - log(J)\right] + \frac{K}{2\phi}\left[log(J\phi)\right]^2. \tag{1}$$

Here, $\mu^0$ is the reference chemical potential for the fluid (solvent), $R$ is the gas constant, $T$ is a constant temperature, $\chi$ is the dimensionless measure of the enthalpy of mixing parameter, $G$ is the shear modulus of the gel polymeric network, $K$ is the bulk modulus of the gel, $J$ is the determinant of the deformation gradient, i.e., $J = det(\boldsymbol{F})$, and $tr(\cdot)$ denotes the trace of a tensor. The first Piola-Kirchhoff stress, $\boldsymbol{P}$, is derived from the free energy using $\boldsymbol{P} = \frac{\partial\Upsilon}{\partial\boldsymbol{F}}$ to obtain the following expression:

$$\boldsymbol{P} = [G(\boldsymbol{F} - \boldsymbol{F}^{-T}) + \frac{K}{\phi}(log(J^e)\boldsymbol{F}^{-T}]. \tag{2}$$

Similarly, the chemical potential is given by $\mu = \frac{\partial\Upsilon}{\partial C_R}$:

$$\mu = \mu^0 + RT(log(1-\phi) + \phi + \chi\phi^2) - \Omega K log(J\phi)[1 - \frac{1}{2}log(J\phi)]. \tag{3}$$

For the fluid flux we assume that the spatial fluid flux, $\boldsymbol{J}$, depends linearly on the spatial gradient of the chemical potential, $\nabla\mu$, so that:

$$\boldsymbol{J} = -M\nabla\mu = -\frac{D}{\Pi\ RT}\left(\frac{1}{\phi - 1}\right)\nabla\mu, \tag{4}$$

where $M$ is the scalar mobility coefficient. Here, $M$ is an isotropic function of the stretch and the fluid concentration (through the polymer volume fraction), and $D$ is the diffusion coefficient.

## 3 DISCRETIZATION TECHNIQUE

The generalized Heaviside-enriched XFEM is adopted to discretize the governing equations [10]. This immersed boundary technique uses enrichment functions on nonconforming meshes to capture spatial discontinuities in elements cut by interfaces. The response for complex geometries and intersection patterns is approximated consistently by allowing for multiple enrichment levels. In this strategy, the state variable field of a two-phase problem is approximated as:

$$\hat{\boldsymbol{\mathcal{U}}}(\boldsymbol{X}) = \sum_{l=1}^{L} \left( H(-\psi) \sum_{i=1}^{n} \mathcal{N}_i \, \hat{\boldsymbol{\mathcal{U}}}_{i,l}^{I} + H(\psi) \sum_{i=1}^{n} \mathcal{N}_i \, \hat{\boldsymbol{\mathcal{U}}}_{i,l}^{II} \right) \tag{5}$$

where $l$ is the enrichment level, $L$ is the maximum number of enrichment levels used for each phase, $\mathcal{N}$ are the shape functions, and $\hat{\boldsymbol{\mathcal{U}}}_{i,l}^{m}$ is the vector of nodal field coefficients, i.e., $\hat{\boldsymbol{\mathcal{U}}} = [\hat{\boldsymbol{u}}, \hat{\mu}]$ at node $i$ for phase $m = I, II$. The hat symbol accent denotes discrete variables. The Heaviside functions, $H$, controls element interpolations in the phases and is defined as: $H(\psi) = 1, \forall\ \psi > 0$; and $H(\psi) = 0, \forall\ \psi \leq 0$. All intersected elements are split into tetrahedral sub-elements via Delaunay triangulation for integration purposes. Note that disconnected domains of identical phase are approximated by different shape functions, and the weak form of the governing equations is only integrated over the corresponding phase in each element; see [10] for details. The flexibility of this approach has been demonstrated extensively ([11, 12]), however, similar immersed techniques that provide a crisp definition of the interface (e.g, CutFem ([9]), and HIFEM ([13])), are equally applicable without loss of generality.

### 3.1 Nodal internal state variables

In the standard finite element method, numerical approximations of ISVs are usually performed pointwise, i.e., per integration point. If this strategy is adopted in immersed boundary analysis methods, the number and location of the ISVs are function of the intersection pattern due to the triangulation. Figure 1a illustrates this scenario in a 2D sketch of an intersected element that requires re-discretization when perturbing the interface. Another drawback of defining ISVs at integration points is that the total number of ISVs can become significantly larger due to the relatively large number of integration points used to integrate intersected elements.

To overcome the aforementioned issues, this paper proposes a conceptually simpler alternative to discretize the ISV fields, namely, define ISVs nodally. In this strategy, ISVs are interpolated by shape functions, similarly to Eq. 5. A set of nodal ISV coefficients, $\hat{\boldsymbol{\phi}}_{\boldsymbol{l}}^{e}$, per enrichment level interpolate the ISV at any point in an element, $e$, for an enrichment level, $l$, by $\phi_l^e(\boldsymbol{X}) = \sum_{k=1}^{N_{nodes}^e} \mathcal{N}_k(\boldsymbol{X})(\hat{\phi}_l^e)_k$. Since inter-element space continuity is not required for the ISVs (see Eq. (9)), nodal ISVs defined at nodes of adjacent elements are not shared, but defined separately for each background element and enrichment level, as seen in Fig. 1b.

Despite the governing equations are evaluated only in the material phase, the state variable fields extend to the unphysical space, i.e., the subdomain of an intersected element on which the governing equations are not defined. There are cases where the value of a state variable field is bounded, such as $0 < \phi < 1$ in the model introduced above. When using a standard finite element interpolation scheme, such as Lagrange functions, the bounds can be satisfied by imposing constraints on the coefficient of the interpolation functions, i.e., the Degrees Of

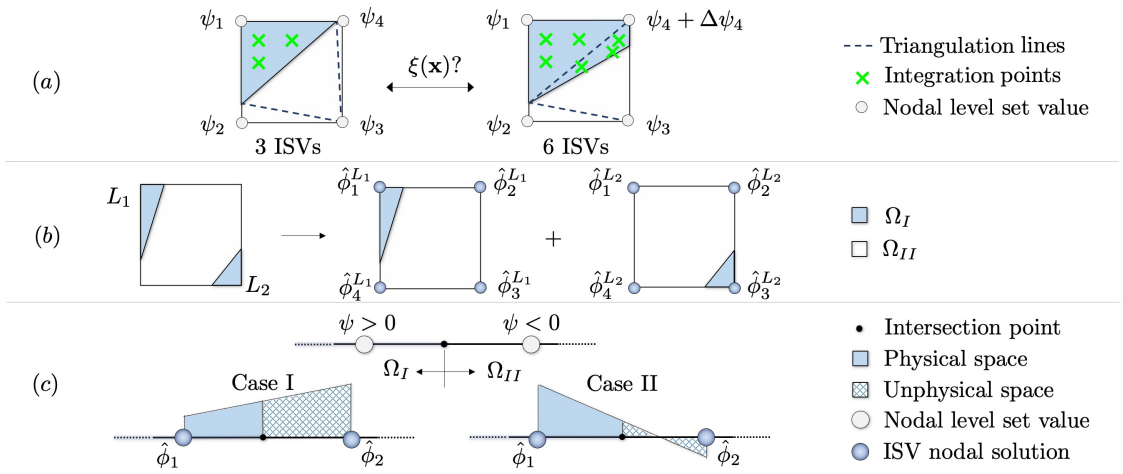


**Figure 1**: Nodal IVS considerations: (a) integration points for different triangulations, (b) independent set of ISVs per enrichment level, and (c) linear interpolation beyond physical space.

Freedom (DOFs). In the case of XFEM this is not possible, as illustrated for a 1D intersected element in Fig. 1c. In this Figure, case II shows that the nodal values on the unphysical space can be negative without producing a negative response in the physical space. To avoid numerical issues associated with ISV values exceeding their bounds in the unphysical space, the ISVs are projected into an unbounded space using $\tilde{\phi} = -log\left(\frac{1}{\phi} - 1\right)$, where $\tilde{\phi}$ is the projected unbounded ISV. This projection is applied to the governing equations formulated below.

### 3.2 Implementation

The weak form the equations governing the hydrogel response can be written as follows:

$$\mathcal{R}_{Gbl} = \begin{bmatrix} \mathcal{R}_{\mathbf{u}^{Gbl}} \\ \mathcal{R}_{\mu^{Gbl}} \end{bmatrix} = \begin{bmatrix} \mathcal{R}_{\mathbf{u}^P} + \mathcal{R}_{\mathbf{u}^I} + \mathcal{R}_{\mathbf{u}^D} + \mathcal{R}_{\mathbf{u}^F} \\ \mathcal{R}_{\mu^P} + \mathcal{R}_{\mu^I} + \mathcal{R}_{\mu^D} + \mathcal{R}_{\mu^F} \end{bmatrix} = \begin{bmatrix} 0 \\ 0 \end{bmatrix}, \qquad \mathcal{R}_{Lcl} = \mathcal{R}_{\phi^P} = 0; \tag{6}$$

where $\mathcal{R}_{Gbl}$ define the global problem that governs the mechanical and chemical state variables, i.e., the $\mathbf{u}$ and $\mu$ unknowns, while the last equation is used to compute the nodal ISVs, $\phi$. The superscript $P$ identifies the residual terms. The superscripts $I$, $D$ and $F$ label the terms used to weakly enforce Dirichlet interface and boundary conditions, and stabilization, respectively. These additional residual terms are explained below. Note that the weakly enforced conditions and stabilization terms are not needed in $\mathcal{R}_{Lcl}$.

#### 3.2.1 Weak form of hydrogel model ($\mathcal{R}_{\mathbf{u}^P}$, $\mathcal{R}_{\mu^P}$, $\mathcal{R}_{\phi^P}$)

The weak form of the governing equations in the absence of body forces and following variational principal is described below. A total Lagrangian formulation and a first order backwards difference implicit scheme are used. The mechanical residual of the transient global problem of this coupled model consists of the balance of momentum defined as:

$$\mathcal{R}_{\mathbf{u}^P}(\mathbf{u}, \phi^*) = \int_{\Omega^I} \delta \boldsymbol{F}(\mathbf{u}) : \boldsymbol{P}(\mathbf{u}, \phi^*) dV - \int_{\Gamma} \delta \mathbf{u} \bar{\boldsymbol{t}} \, d\Gamma. \tag{7}$$

Similarly, the balance of the mass of the solvent is as follows:

$$\mathcal{R}_{\mu^P}(\mu,\phi^*,\phi^{*(n-1)}) = -\int_{\Omega^I}\delta\mu\left[\frac{1-\phi^{*(n-1)}/\phi^*}{\Delta t\ \Omega\phi^*}\right]dV + \int_{\Omega^I}\delta\mu\boldsymbol{J}(\mu,\phi^*)\ dV + \int_{\Gamma}\delta\mu\bar{j}\ d\Gamma. \tag{8}$$

In these residuals, $\delta\mathbf{u}$ and $\delta\mu$ are kinematically admissible displacement and chemical potential test functions, respectively. Here, the previous time step with time increment $\Delta t$ is denoted by the superscript $(n-1)$, and the asterisk on the ISVs, i.e., $\phi^*$, indicates equilibrium. Thus, both the stress, $\boldsymbol{P}$, and the flux, $\boldsymbol{J}$, are function of the ISV variables at local equilibrium. Moreover, the chemical residual is also function of the previous state of the ISVs.

For given state variables $\mathbf{u}$ and $\mu$, the ISV $\phi$ is governed by the following residual:

$$\begin{aligned}\mathcal{R}_{\phi^P}(\mathbf{u},\mu) = &\int_{\Omega^e}\delta\phi\left\{\frac{\mu^0-\mu}{RT} + log(1-\phi) + \phi + \chi(\phi)^2 - \frac{\Pi K}{RT}\left[log(J\phi)\left(1+\frac{1}{2}log(J\phi)\right)\right]\right\}\ dV \\ &+ \int_{\Omega^e}\delta\nabla\phi\nabla\phi\left\{\frac{1}{\phi-1} + 1 + 2\chi\phi - \frac{\Pi K}{RT\phi}\left[1-log(J\phi)\right]\right\}\ dV.\end{aligned} \tag{9}$$

Similarly, $\delta\phi$ is a kinematically admissible ISV test function, but integrated over an element domain, $\Omega^e$, as described in 3.1. Note that Eq. (9) has been augmented with a stabilization term following the Galerkin Gradient Least-Squares (GGLS) approach to mitigate the generation of wiggles or oscillations in the solution ([14]). The GGLS method is preferred for stability in the $H1$ semi-norm, i.e., to enforce continuity in the spatial gradient of the ISV residual and thus, preserve consistency with the global problem.

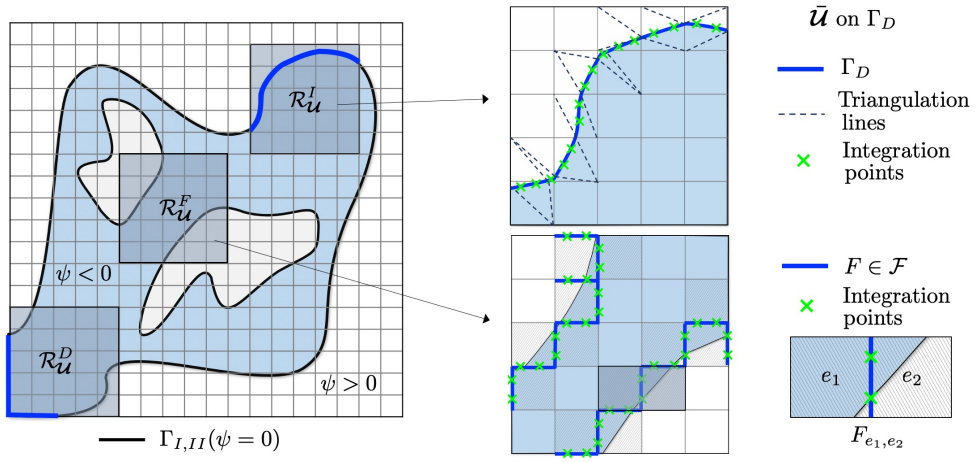


**Figure 2**: Illustration of a 2D domain described by a level set field together with sketches of the strategies for weakly enforce boundary and interface conditions ($\mathcal{R}_{\mathcal{U}^D}$, $\mathcal{R}_{\mathcal{U}^I}$) and ghost penalization ($\mathcal{R}_{\mathcal{U}^F}$).

### 3.2.2 Interface and boundary conditions ($\mathcal{R}_{\mathbf{u}^I}$, $\mathcal{R}_{\mathbf{u}^D}$, $\mathcal{R}_{\mu^I}$, $\mathcal{R}_{\mu^D}$)

In the problem configurations considered here, an initially dry hydrogel swells due to the continuous supply of solvent modeled by a varying chemical potential prescribed along either the

interface and/or external boundaries. In the XFEM framework presented previously, Neumann conditions are prescribed the same way as in standard finite elements. Dirichlet interface and external boundary conditions, however, are enforced weakly via the unsymmetric version of Nitsche's method [15]. In the proposed formulation, the residual terms are function of the ISVs and the state variables, and second order derivatives of the stress and flux are required for a consistent formulation (i.e., an exact Jacobian/Tangent):

$$\begin{aligned}\mathcal{R}_{\mathbf{u}^I}(\mathbf{u},\phi^*) &= -\int_\Gamma \delta\mathbf{u}\boldsymbol{P}(\mathbf{u},\phi^*)\boldsymbol{\eta}\ d\Gamma \mp \int_\Gamma \delta\boldsymbol{P}(\mathbf{u};\delta\mathbf{u},\phi^*)\boldsymbol{\eta}\ [\![\mathbf{u}]\!]\ d\Gamma + \int_\Gamma \left(\frac{1}{\phi}\right)\frac{G}{h}\gamma_u^D\ [\![\delta\mathbf{u}]\!]\ [\![\mathbf{u}]\!]\ d\Gamma,\\ \mathcal{R}_{\mu^I}(\mu,\phi^*) &= -\int_\Gamma \delta\mu\boldsymbol{J}(\mu,\phi^*)\boldsymbol{\eta}\ d\Gamma \mp \int_\Gamma \delta\boldsymbol{J}(\mu;\delta\mu,\phi^*)\boldsymbol{\eta}\ [\![\mu]\!]\ d\Gamma + \int_\Gamma \left(\frac{1}{\phi}-1\right)\frac{M}{h}\gamma_\mu^D\ [\![\delta\mu\ ]\!][\![\mu]\!]\ d\Gamma.\end{aligned} \tag{10}$$

The jump operator $[\![\cdot]\!]$ is defined as $[\![\boldsymbol{\mathcal{U}}(\mathbf{X})]\!] = \lim_{\epsilon\to 0^+}\boldsymbol{\mathcal{U}}(\mathbf{X}+\epsilon) - \boldsymbol{\mathcal{U}}(\mathbf{X}-\epsilon) = \boldsymbol{\mathcal{U}}(\mathbf{X}) - \bar{\boldsymbol{\mathcal{U}}}$. The vector $\boldsymbol{\eta}$ represents the normal of the interface. The penalty factors to enforce the prescribed Dirichlet boundary conditions $\bar{\boldsymbol{u}}$ and $\bar{\mu}$ are denoted by the penalty factors, $\gamma_{\mathbf{u}}^D$ and $\gamma_\mu^D$, respectively. To include the transient effect of the ISVs, the last terms are multiplied by a factor function of the ISVs. Note that a dry and wet gel at equilibrium is described by $\phi \approx 0.999$ and $\phi \approx [0.1 - 0.2]$, respectively, which circumvents numerical issues arising from division by zero.

### 3.2.3 Face-oriented ghost stabilization ($\mathcal{R}_{\mathbf{u}^F}$, $\mathcal{R}_{\mu^F}$)

Numerical instabilities can occur in the XFEM (and similar immersed boundary analysis techniques) when the material interface moves too close to a node of the background mesh. Such configurations lead to a vanishing zone of influence of certain DOFs. In this work, the face-oriented ghost penalization proposed by [16] is used in the vicinity of the interface to stabilize the XFEM discretization:

$$\begin{aligned}\mathcal{R}_{\mathbf{u}^F}(\mathbf{u},\phi^*) &= \sum_{F\in\mathcal{F}}\int_\Gamma \left(\frac{1}{\phi}\right) Gh\gamma_{\mathbf{u}}^G\ [\![\delta\nabla\mathbf{u}\ \boldsymbol{\eta}]\!]\ [\![\boldsymbol{P}(\mathbf{u},\phi^*)\ \boldsymbol{\eta}]\!]\ d\Gamma,\\ \mathcal{R}_{\mu^F}(\mu,\phi^*) &= \sum_{F\in\mathcal{F}}\int_\Gamma \left(\frac{1}{\phi}-1\right) Mh\gamma_\mu^G\ [\![\delta\nabla\mu\ \boldsymbol{\eta}]\!]\ [\![\boldsymbol{J}(\mu,\phi^*)\boldsymbol{\eta}]\!]\ d\Gamma.\end{aligned} \tag{11}$$

The faces $F$ in the set $\mathcal{F}$ are the element faces in the vicinity of the interface for which at least one of the two adjacent elements is intersected as shown in the onset of Fig. 2. The normals of the shared elements are denoted by $\boldsymbol{\eta}$. Similar to the previous section, both residuals are scaled by factors functions of the ISVs to account for the transient response.

## 4 NUMERICAL APPROACH

### 4.1 Adaptive time increment scheme

A pseudo time continuation method is used to reach steady state. The time increment is updated using $\Delta t = f_{\Delta t}\Delta t^{(n-1)}$. The parameter, $f_{\Delta t}$, is chosen to be greater than one when the Newton algorithm converges. Conversely, if either the local or global problem diverges, the current time increment is restarted with $f_{\Delta t} < 1$. Numerical experiments show that choosing

$f_{\Delta t} = [0.5 - 1.15]$ allows the problem to converge to steady state without an excessive number of time increments.

In the first phase of this transient problem, rearrangement of molecules in the gel due to the inflow of solvent occurs in a relatively small time. In this stage, the problem is dominated by its chemical component and little swelling occurs. Thus, a small time increment is needed to capture this. Subsequently, once a considerable amount of solvent has been absorbed by the gel, large deformations controlled by the mechanical component require time steps that are orders of magnitude larger than the first stage of this process to reach steady state. However, if the time increment is too large, numerical instabilities associated with excessive swelling may compromise convergence. Hence, a geometric progression of the time increment is used.

### 4.2 Nested Newton scheme

Unknowns at each discrete time are computed according to the nested Newton scheme ([17]), where the global problem of the states of the model is decoupled from the local problem that defines the evolution of the ISVs. This implies that the residuals in Eq. (9) are solved prior to the construction of the elemental mechanical and chemical residuals. Hence, two Newton loops are needed to solve this problem: an inner Newton loop that solves the nonlinear local problem $\mathcal{R}_{Lcl} = 0$, per element of the background mesh and level of enrichment; and an outer Newton loop to compute the solution of $\mathcal{R}_{Gbl} = [\mathcal{R}_{\mathbf{u}^{Gbl}},\ \mathcal{R}_{\mu^{Gbl}}]^T = \mathbf{0}$ globally. The state variables $\mathbf{u}$ and $\mu$ are assumed to be constant in the local problem. The converged ISVs are used in the consistent linearization of the global problem.

The second-order derivatives required for weakly imposing Dirichlet boundary and interface conditions involve additional explicit and implicit dependencies of the nodal ISVs. Hence, $\frac{d^2\mathcal{R}_{Lcl}}{d\mathbf{u}^2}$, $\frac{d^2\phi}{d\mathbf{u}^2}$, $\frac{d^2\mathcal{R}_{Lcl}}{d\mu^2}$, $\frac{d^2\phi}{d\mu^2}$, $\frac{d^2\mathcal{R}_{Lcl}}{d\mu d\mathbf{u}}$, $\frac{d^2\phi}{d\mu d\mathbf{u}}$. are also needed, which results in considerably higher memory requirements and operations on higher-order tensors. Adding these derivatives implies additional non-traditional operators of higher-order derivations from intricate nonlinear expressions. Note that if the projection of the ISVs is used, the derivative between the projected and unprojected ISVs (i.e., $\frac{\partial\phi}{\partial\tilde{\phi}} = \frac{2}{\pi(\tilde{\phi}^2+1)}$ and $\frac{\partial^2\phi}{\partial\tilde{\phi}^2} = \frac{-4\tilde{\phi}}{\pi(\tilde{\phi}^2+1)^2}$) should also be included.

### 4.3 Model nondimensionalization

To ameliorate numerical instabilities due to the significant difference in magnitude between the mechanical and chemical solutions, the governing equations are nondimensionalized. The nondimensional problem is constructed using two independent parameters: a reference length, $L_{ref}$, and a reference chemical potential, $\mu_{ref}$. The parameter $L_{ref}$ is the scaling factor between the nondimensional mesh and the actual domain size. The initial prescribed chemical potential (which represents a dry hydrogel gel) is used for $\mu_{ref}$. A tilde is added on the symbols used for the nondimensional parameters to differentiate them from their dimensional counterparts. To nondimensionalize the model in a non-invasive manner, i.e., keep the original formulation intact and only modify material parameters, the following must be satisfied: $\frac{G_{ref}}{L_{ref}} = 1$ and $\frac{D_{ref}G_{ref}}{\mu_{ref}L_{ref}^2} = \frac{D_{ref}}{\mu_{ref}L_{ref}} = 1$. Hence, after replacing these two equalities into the the nondimensional expressions, the hydrogel model parameters are obtained using the following expressions: $t = \frac{L_{ref}}{D_{ref}}\tilde{t}$, $D_{ref} = \mu_{ref}L_{ref}$, $\Omega = \Omega_{ref}\tilde{\Omega}$, $\Omega_{ref} = \frac{\mu_{ref}}{G_{ref}}$, $D = D_{ref}\tilde{D}$, $RT = \mu_{ref}\tilde{RT}$. The state

variables are recovered using $u = L_{ref}\tilde{u}$, and $\mu = \mu_{ref}\tilde{\mu}$.

## 5 NUMERICAL EXAMPLES

The following examples demonstrate the applicability of the proposed immersed analysis framework considering open systems thermodynamic. To precipitate the supply of solvent to the hydrogel, an exponentially varying in time chemical potential is prescribed along boundaries. The chemical potential is a function of the total simulation time and decreases orders of magnitude throughout the swelling process until it reaches a value of zero using $\bar{\mu}(t) = \mu_0 + \bar{\mu}_0\ e^{-\frac{t}{t_\mu}}$, with $t = \sum_{i=0}^{n-1} \Delta t^{(i)}$. The reference chemical potential of the surrounding solvent is set to zero, i.e., $\mu_0 = 0\ J/mol$. The parameter $\bar{\mu}_0$ represents the initial, uniform chemical potential of a dry hydrogel. Typically, a relatively large negative value, i.e., $\bar{\mu}_0 \approx [-10^4, -10^5]\ J/mol$, is used. The parameter $t_\mu$ offers control on the exponential decay of the chemical potential and thus, the speed of the absorption of solvent by the hydrogel. In the problems explored in this paper, this parameter is set in the range of $t_\mu = [150 - 500]s$. In addition, mechanical boundary conditions (prescribed displacements and tractions) are enforced as specified in each example. Material properties are summarized in Table 1 in SI units. Initial chemical and ISV conditions are also included.

**Table 1**: Material properties and initial conditions of hydrogel model

| Description | Symbol | Value [Units] |
|---|---|---|
| Shear Modulus | $G$ | 1.0x10$^6$[$Pa$] |
| Bulk Modulus | $B$ | 1.0x10$^8$[$Pa$] |
| Diffusion coefficient | $D$ | 5.0x10$^{-5}$[$m^2/s$] |
| Enthalpy of mixing | $\chi$ | 0.2[$-$] |
| Temperature | $T$ | 21 [C] |
| Initial chemical potential | $\bar{\mu}_0$ | $-1.48 \times 10^4$[$J/mol$] |
| Initial polymer volume fraction | $\bar{\phi}_0$ | 0.999[$-$] |

Note that the accuracy of the proposed XFEM framework was verified in 2D and 3D against numerical results using standard finite elements, which has been omitted for brevity.

### 5.1 Example 1: free swelling

An eighth of a nondimensional cubic domain of edge length 1.0 with a spherical inclusion located at the center is consider to simulate free swelling, see Fig. 3a. An exponentially decaying chemical potential is prescribed along the top, right and back faces which are not intersected by the inclusion. Furthermore, symmetry conditions are enforced along the bottom, left and front faces. The radius of the hole is set to be half of the height of the domain. The problem domain is discretized by a $10 \times 10 \times 10$ mesh.

Figure 3b shows snapshots of deformed configuration (without scaling) colored by the ISV field to visualize the evolution of the free swelling problem. This simulation highlights three of the main characteristics of hydrogel analysis. First, the final simulation time is orders of magnitude larger than the initial time step, as reported on the top. Second, the swelling of hy-

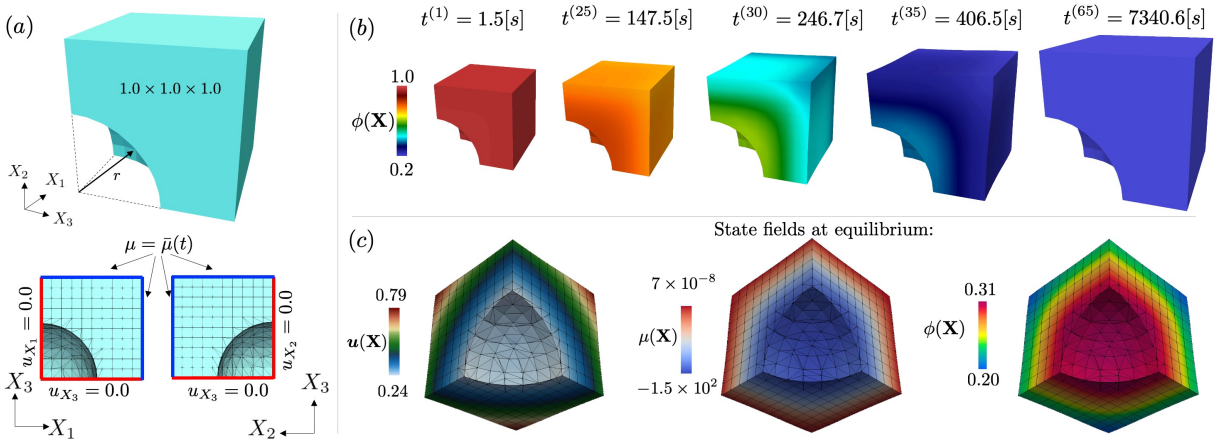


**Figure 3**: (Left) Problem setup: free swelling of cube with spherical hole; (top-right) Evolution of gel shape; (bottom-right) state fields of final time increment.

drogels is non-uniform at intermediate stages of the transient response. And third, the swollen hydrogel at the end of the simulation is considerably larger than the initial configuration. The displacement reaches values in the order of the domain size, while the chemical potential decreases exponentially, as shown in Figure 3c. Note that for visualization purposes only, the nodal values are averaged to produce a continuous nodal ISV field. Overall, the augmented residual with stabilization and weakly enforced conditions components is able to accurately predict the hydrogel's response in benchmark-like 3D tests.

### 5.2 Example 2: constrained swelling

To demonstrate the robustness of this XFEM framework in terms of being able to predict physical instabilities, the example described in [6] is reproduced here. The reader is referred to [6] for details of the problem configuration. In this example, a hydrogel ring has an influx of solvent through the top face. The displacement of the bottom face is constrained in all directions. The zero isocontour of the level set field slices the top face to produce small random geometric imperfections to aid the initiation of buckling, see [6]. Two different thicknesses are considered to simulate a "thick" and a "thin" ring. The other parameters remain unchanged in both configurations.

Figure 4 shows snapshots of the evolution of the shapes of the constrained gels, colored by the ISV field. The change in thickness leads to drastically different swollen shapes, i.e., the top one stable with an axisymmetrically swollen gel, and the bottom one with a buckled pattern. These results resemble those observed in experiments.

## 6 CONCLUSIONS

- An XFEM approach to simulate hydrogels was introduced. The model used couples large deformations and nonlinear diffusion where the local material response is described by a gradient-independent ISV that defines the swelling state. ISVs are interpolated by shape functions for each element and enrichment level and projected into an unbounded space.

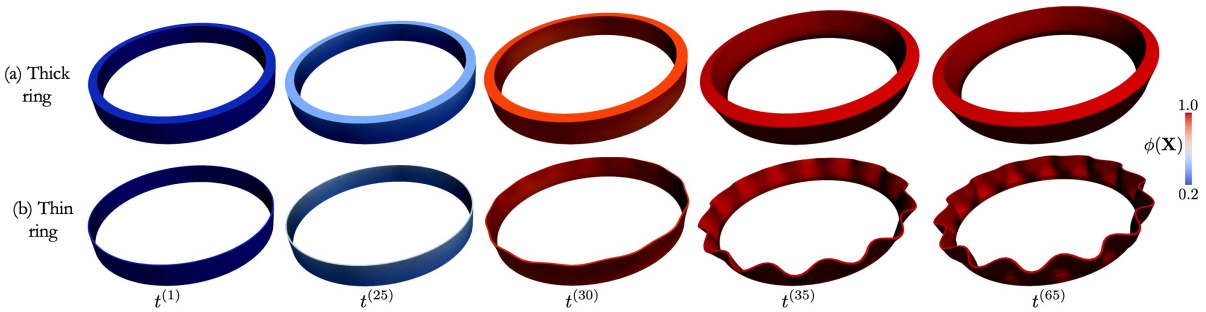


**Figure 4**: Evolution of constrained swelling of (top) thick ring and (bottom) thin ring.

- The formulations to weakly enforce boundary and interface conditions, and to stabilize gradients in the vicinity of the interface, were augmented to include the transient effect of the ISVs. A pseudo transient continuation scheme was introduced to solve for steady state conditions. This scheme involves nested Newton solvers for the global and local problems.

- The XFEM approach was verified with two problems considering free and constrained swelling of the hydrogel. The supply of solvent to the gel is simulated via a time-dependent chemical potential that is prescribed at external boundaries and interfaces. The problems showed the large deformation nature of hydrogels, as well as the non-uniform swelling behavior of the transient response.

- Future work should include the application of the presented approach to other problems that require the use of models with ISVs such as elastoplasticity. Moreover, the robustness of this framework should be tested in configurations that will benefit from the ISV interpolation scheme introduced here, e.g., design optimization problems using the methods described in [18]. These methods require computation of gradients with respect to shape and topology optimization parameters and thus, are affected by how ISVs are defined.

## 7 ACKNOWLEDGEMENTS

All authors acknowledge the support of the National Science Foundation (CMMI-1463287). The first author acknowledges partial auspice of the U.S. Department of Energy by Lawrence Livermore National Laboratory under Contract DE-AC52-07NA27344 (LLNL-PROC-834090).

## REFERENCES

[1] Coleman, B. D. and Gurtin, M. E. *Thermodynamics with internal state variables.* The Journal of Chemical Physics 47 (2) (1967) 597–613.

[2] de Borst, R. *Challenges in computational materials science: multiple scales, multi-physics and evolving discontinuities.* Computational Materials Science 43 (1) (2008) 1–15.

[3] Mao, Y. and Ding, Z. and Yuan, C and Ai, S. and Isakov, M and Wu, J. and Wang, T. and Dunn, M. L. and Qi, H. J. *3d printed reversible shape changing components with stimuli responsive materials.* Scientific reports 6 (2016) 24761.

[4] Chester, S. A. and Anand, L. *A coupled theory of fluid permeation and large deformations for elastomeric materials*. Journal of the Mech and Phy of Solids 58 (11) (2010) 1879–1906.

[5] Simo, J. C. *A framework for finite strain elastoplasticity based on maximum plastic dissipation and the multiplicative decomposition: Part i. continuum formulation*. CMAME 66 (2) (1988) 199–219.

[6] Chester, S. A., Claudio, V. and Lallit A. *A finite element implementation of a coupled diffusion-deformation theory for elastomeric gels*. International Journal of Solids and Structures 52 (2015): 1-18.

[7] Benvenuti, E. *A regularized XFEM framework for embedded cohesive interfaces*. Computer Methods in Applied Mechanics and Engineering 197 (49-50) (2008) 4367–4378.

[8] Duysinx, P. and Miegroet, L. and Jacobs, T. and Fleury, C. *Generalized shape optimization using X-FEM and level set methods*. In: IUTAM Symposium on Topological Design Optimization of Structures, Machines and Materials, Springer, 2006, pp. 23–32.

[9] Burman, E. and Claus, S. and Hansbo, P. and Larson, M. G., and Massing, A. *CutFEM: discretizing geometry and partial differential equations*. International Journal for Numerical Methods in Engineering 104 (7) (2015) 472–501.

[10] Makhija, D. and Maute, K. *Numerical instabilities in level set topology optimization with the extended finite element method*. Struct and Multidiscip Opt 49 (2) (2014) 185–197.

[11] Barrera, J. L. and Geiss, M. J. and Maute, K. *Hole seeding in level set topology optimization via density fields*. Structand Multidiscip Opt 61.4 (2020): 1319-1343.

[12] Barrera, J. L. and Maute, K. *Ambiguous phase assignment of discretized 3D geometries in topology optimization*. CMAME 369 (2020): 113201.

[13] Soghrati, S. and Barrera, J. L. *On the application of higher-order elements in the hierarchical interface-enriched finite element method* International Journal for Numerical Methods in Engineering 105 (6) (2016) 403–415.

[14] Franca, L. P. and Gomes Dutra Do Carmo, E. *The Galerkin gradient least-squares method*. Computer Methods in Applied Mechanics and Engineering 74.1 (1989): 41-54.

[15] Hansbo, A. and Hansbo, P. *A finite element method for the simulation of strong and weak discontinuities in solid mechanics*. CMAME 193 (33) (2004) 3523–3540.

[16] Burman, E. and Claus, S. Hansbo, P. Larson, M. G. and Massing, A. *CutFEM: discretizing geometry and partial differential equations*. International Journal for Numerical Methods in Engineering 104 (7) (2014) 472–501.

[17] Simo, J. C. and Taylor, R. L. *Consistent tangent operators for rate-independent elastoplasticity*. CMAME 48 (1) (1985) 101–118.

[18] Sigmund, O. and Maute, K. *Topology optimization approaches*. Structural and Multidisciplinary Optimization 48.6 (2013): 1031-1055.